



OPEN

## Effects of urban functional fragmentation on nitrogen dioxide (NO<sub>2</sub>) variation with anthropogenic-emission restriction in China

Yuan Meng<sup>1</sup>, Man Sing Wong<sup>1,2</sup>✉, Hanfa Xing<sup>3,4</sup>, Rui Zhu<sup>1</sup>, Kai Qin<sup>5</sup>, Mei-Po Kwan<sup>6,7</sup>, Kwon Ho Lee<sup>8</sup>, Coco Yin Tung Kwok<sup>1</sup> & Hon Li<sup>1</sup>

Urban functional fragmentation plays an important role in assessing Nitrogen Dioxide (NO<sub>2</sub>) emissions and variations. While the mediated impact of anthropogenic-emission restriction has not been comprehensively discussed, the lockdown response to the novel coronavirus disease 2019 (COVID-19) provides an unprecedented opportunity to meet this goal. This study proposes a new idea to explore the effects of urban functional fragmentation on NO<sub>2</sub> variation with anthropogenic-emission restriction in China. First, NO<sub>2</sub> variations are quantified by an Autoregressive Moving Average with external variables-Dynamic Time Warping (SARIMAX-DTW)-based model. Then, urban functional fragmentation indices including industrial/public Edge Density (ED) and Landscape Shape Index (LSI), urban functional Aggregation Index (AI) and Number of Patches (NP) are developed. Finally, the mediated impacts of anthropogenic-emission restriction are assessed by evaluating the fragmentation-NO<sub>2</sub> variation association before and during the lockdown during COVID-19. The findings reveal negative effects of industrial ED, public LSI, urban functional AI and NP and positive effects of public ED and industrial LSI on NO<sub>2</sub> variation based on the restricted anthropogenic emissions. By comparing the association analysis before and during lockdown, the mediated impact of anthropogenic-emission restriction is revealed to partially increase the effect of industrial ED, industrial LSI, public LSI, urban functional AI and NP and decrease the effect of public ED on NO<sub>2</sub> variation. This study provides scientific findings for redesigning the urban environment in related to the urban functional configuration to mitigating the air pollution, ultimately developing sustainable societies.

### Abbreviations

NO <sub>2</sub>	Nitrogen Dioxide
AQI	Air Quality Index
PM <sub>2.5</sub>	Fine particulate matter with a diameter less than 2.5 μm
PM <sub>10</sub>	Particulate matter with a diameter of less than 10 μm (PM <sub>10</sub> ),
O <sub>3</sub>	Ozone
SO <sub>2</sub>	Sulfur Dioxide
CO	Carbon Monoxide

<sup>1</sup>Department of Land Surveying and Geo-Informatics, The Hong Kong Polytechnic University, Hung Hom, Hong Kong. <sup>2</sup>Research Institute for Sustainable Urban Development, The Hong Kong Polytechnic University, Hung Hom, Hong Kong. <sup>3</sup>School of Geography, South China Normal University, Guangzhou, Guangdong, China. <sup>4</sup>College of Geography and Environment, Shandong Normal University, Jinan, Shandong, China. <sup>5</sup>School of Environment and Spatial Informatics, China University of Mining and Technology, Xuzhou, China. <sup>6</sup>Department of Geography and Resource Management, and Institute of Space and Earth Information Science, The Chinese University of Hong Kong, Sha Tin, Hong Kong. <sup>7</sup>Department of Human Geography and Spatial Planning, Utrecht University, 3584 CB Utrecht, The Netherlands. <sup>8</sup>Department of Atmospheric and Environmental Sciences, Gangneung-Wonju National University, Gangneung 25457, South Korea. ✉email: Ls.charles@polyu.edu.hk

COVID-19	Novel coronavirus disease 2019
SARIMAX-DTW	Autoregressive Integrated Moving Average with external variables-Dynamic Time Warping
ED	Edge Density
LSI	Landscape Shape Index
AI	Aggregation Index
NP	Number of Patches
PLADJ	Percentage of Like Adjacencies
NP	Number of Patches
COHESION	Patch Cohesion Index
UFB	Urban functional Fragmentation characteristics Before lockdowns
UFD	Urban functional Fragmentation characteristics During lockdowns
UFCB	Urban functional Fragmentation characteristics and Controlling variables Before lockdowns
UFGD	Urban functional Fragmentation characteristics and Controlling variables During lockdowns
GAMs	Generalized Additive Models
VIF	Variance Inflation Factor
CI	Confidence-Interval
CNEMC	China National Environmental Monitoring Center
CMA	China National Meteorological Science Data Center
AIC	Akaike Information Criterion

Urban functional fragmentation refers to the breaking up of urban functional areas, such as residential and industrial lands, into more isolated segments<sup>1,2</sup>. It encourages diverse human activities such as vehicular mobility and large quantities of manufactures, result in the diversity and vulnerable fractions of urban function areas and cause a series of anthropogenic pollution such as noise and air pollutants<sup>3,4</sup>. Nitrogen Dioxide (NO<sub>2</sub>) has been considered as one of the major anthropogenic emissions<sup>5,6</sup>, which is associated with several social environmental issues, such as cardiopulmonary mortality<sup>7</sup>, lung cancer<sup>8</sup> and severe air pollution<sup>9</sup>. The anthropogenic emissions of NO<sub>2</sub> are mainly attributed by fossil fuel uses from various urban functions such as traffic, industrial and public uses<sup>10</sup>. Evaluating the impact of urban functional fragmentation is essential to estimate NO<sub>2</sub> emissions.

The rapid emergence of the novel coronavirus disease 2019 (COVID-19) has significantly changed the business-as-usual circumstance of the anthropogenic NO<sub>2</sub> emissions<sup>11</sup>. Due to the policies of lockdowns and restricted social distancing proposed by the governments, the regular socioeconomic activities are drastically reduced<sup>12</sup>, leading to the variation of anthropogenic-generated emissions<sup>13–15</sup>. These changes have brought opportunities to estimate the impact of urban functional fragmentation under different circumstances of NO<sub>2</sub> emissions, i.e. the differences between NO<sub>2</sub> emissions before and after lockdowns<sup>16,17</sup>. For instance, the lockdowns have significantly reduced the traffic flows, which tend to exceed the road capability before lockdowns, and thus change the influence of roads with heavy traffics on NO<sub>2</sub> emissions<sup>18–20</sup>.

Current studies on the association analysis between urban functional fragmentation and NO<sub>2</sub> concentration can be reviewed based on three main aspects, including the air pollution metrics, fragmentation metrics and the methods for association analysis. For quantifying NO<sub>2</sub> emissions, existing approaches can be divided into two aspects, including the total column-based and difference-based quantification. The total column-based NO<sub>2</sub> quantification, involving hourly, daily, monthly and annual concentration, has been utilized to depict the temporal variation of NO<sub>2</sub><sup>21–23</sup>. For instance, Li, et al.<sup>23</sup> proposed multiple dimensions including hourly average values, daily average values and the standard deviation of the peak hours to depict the variation of NO<sub>2</sub> concentrations. However, such approach only quantifies the NO<sub>2</sub> changes within the research period and cannot evaluate the historical NO<sub>2</sub> trends that may be drastically different from the research-period trends caused by unprecedented events, i.e. COVID-19. To fill this gap, difference-based quantification has been utilized to depict such historical-research period changes of COVID-19. For instance, Venter, et al.<sup>16</sup> defined the NO<sub>2</sub> differential as the difference between the NO<sub>2</sub> concentration in the research period and the average values of the historical three-year baseline.

For the fragmentation metrics for depicting urban functions, both specific metric and urban functions that are highly associated with anthropogenic air pollutant emissions are concerned. In particular, basic quantifications of urban functional areas, including edge length, patch areas, and their synthetical characteristics of fragmentation such as landscape shape index (LSI) and Aggregation Index (AI), Percentage of Like Adjacencies (PLADJ), Number of Patches (NP), Patch Cohesion Index (COHESION), impervious area-weighted mean shape index and contiguity index, have been utilized to estimate the variations of air pollutants<sup>22,24–27</sup>. Moreover, research has indicated that industrial and public functions, as well as the mixture of urban functions, which are highly related to the use of energy resources such as fuels, minerals and electric power, show a higher impact on anthropogenic air pollution emissions<sup>28–30</sup>. He, et al.<sup>31</sup> have indicated the positive trends between the industrial functional fragmentation and NO<sub>2</sub> concentrations. Research has also revealed that the distribution of public urban functions including greenery and parks show the potential to influence NO<sub>2</sub> variations<sup>32,33</sup>.

For association analysis, regression models such as ordinary least squares, spatial autoregressive model and panel data model have been considered. Lee<sup>34</sup> adopted ordinary least squares and two-level regression models to control geographic and metropolitan-level socioeconomic factors for urban form estimation, and further indicated that high-level urban function mixing shows the potential to reduce air pollutant emissions. Li and Zhou<sup>35</sup> involved the spatial correlation of urban fragmentation characteristics and applied the spatial autoregressive

model, suggesting that scattered polycentric cities in China are associated with better air quality. Panel data analysis has also been utilized to quantify the link between urban forms and air pollution, revealing negative association between urban fragmentation and air quality<sup>36</sup>.

Despite of the above discussed approaches in existing studies, limitations still exist faced with the emergence of COVID-19<sup>37–40</sup>. First, although extracting the average value in the difference-based quantification concerns the historical NO<sub>2</sub> variation, the changes of the historical NO<sub>2</sub> concentration is ignored. For instance, the three-year average NO<sub>2</sub> values cannot depict the potential changes among these years. Thus, effective approaches of quantifying the overall temporal trends of NO<sub>2</sub> concentration is required. In addition, the lag effect should be considered in the difference-based quantification to avoid the biases caused by the point-to-point (such as day-to-day measurement) differential calculation. Second, considering that most human activities including business and leisure have been significantly changed by the COVID-19, the fragmentation depiction should focus on the industrial and public related urban functions. The synthetical urban functional characteristics also need be concerned to implement the overall urban functional fragmentation quantification. Third, despite that multi-perspective covariates such as meteorological and spatial factors have been concerned in previous research, different scenarios of anthropogenic emissions during COVID-19 caused by the lockdown policies are not fully considered in evaluating the impact of urban functional fragmentation.

Meanwhile, among the countries and regions for analysis, China has experienced drastic industrialization and urbanization<sup>41,42</sup>, leading to increasing urban population and gross domestic production among cities<sup>43,44</sup>. During this process, urban landscapes and configurations in China have changed dramatically to improve urbanization process<sup>45,46</sup>. Existing studies have found that this rapid transformation of urban forms in China is highly associated with air pollution emissions<sup>47</sup>. Recently, due to the COVID-19, the coronavirus quarantine proposed in China has led to economic slowdown<sup>48</sup>, causing drastic decline of anthropogenic emissions and the variation of NO<sub>2</sub> than ever before<sup>49,50</sup>. The urbanization process and NO<sub>2</sub> changes in the lockdown period in China have provided opportunities to explore the impact of urban functional fragmentation on NO<sub>2</sub> variations based on different scenarios of anthropogenic emissions.

To fill with these gaps, this paper investigates the impact of urban functional fragmentation on NO<sub>2</sub> variation mediated by the changes of anthropogenic air pollutant emissions in China during COVID-19. The objective of this study is (1) to quantify the differential of temporal NO<sub>2</sub> during COVID-19 compared with NO<sub>2</sub> in normal days based on the historical NO<sub>2</sub> trends and the potential lag effects; (2) to depict both single-functional and synthetical-functional fragmentation characteristics driven by the changes of human activities; and (3) to investigate the association between urban functional fragmentation and NO<sub>2</sub> variation based on the different scenarios of anthropogenic emissions during COVID-19.

To achieve the objectives, a new research framework is proposed as follows (Fig. 1). First, an Autoregressive Integrated Moving Average with external variables-Dynamic Time Warping (SARIMAX-DTW)-based model is proposed to quantify NO<sub>2</sub> variations. Then, human activity-driven metrics are considered, including industrial/public Edge Density (ED) and LSI and urban functional AI and NP, to depict fragmentation characteristics of urban functions. Finally, to different scenarios of NO<sub>2</sub> emissions, four models including Urban functional Fragmentation characteristics Before lockdowns (UFB)-based model, Urban functional Fragmentation characteristics During lockdowns (UFD)-based model, Urban functional Fragmentation characteristics and Controlling variables Before lockdowns (UFCB)-based model and Urban functional Fragmentation characteristics and Controlling variables During lockdowns (UFCD)-based model are proposed based on the Generalized Additive Models (GAMs). This study will gain a better understanding of functional fragmentation-NO<sub>2</sub> variation relationship when considering different scenarios of anthropogenic emissions and will help government provide effective guidelines in policy-making to develop sustainable societies.

## Results

**NO<sub>2</sub> variation during COVID-19 epidemic.** Figure 2 reveals the mean observed-predicted error of NO<sub>2</sub> prediction in 145 air stations among three time periods, (1) from Jan. 1st, 2015 to Nov. 1st, 2019, (2) from Jan. 1st, 2015 to Dec. 1st, 2019 and (3) from Jan. 1st, 2015 to Jan. 1st, 2020. Despite of the differential in time periods, similar distributions mean observed-predicted error are observed within 20–40%. It indicates that no significant impacts of time period division are shown on the NO<sub>2</sub> prediction. As we intend to predict NO<sub>2</sub> concentrations during COVID-19 (from Jan. 2020), NO<sub>2</sub> from Jan. 1st, 2015 to Jan. 1st, 2020 were chosen for SARIMAX modeling and those from Jan. 1st, 2020 to May. 1st, 2020 were utilized for prediction.

On this basis, temporal NO<sub>2</sub> concentrations in 145 air stations during Jan. 1st, 2020 to May 1st, 2020 were utilized as testing data in SARIMAX models. The prediction of NO<sub>2</sub> concentration of 145 air stations is shown in Fig. S1. In particular, Fig. 3 displays two selected air stations to illustrate the predicted NO<sub>2</sub> patterns. Red lines and blue lines represent the overall temporal trends of observed and predicted NO<sub>2</sub> concentrations, respectively. In particular, the predicted NO<sub>2</sub> trends are consistent with the periodical patterns of historical NO<sub>2</sub> before Jan. 1st, 2020. Lower NO<sub>2</sub> concentrations are shown on the observed NO<sub>2</sub> trends compared with the predicted ones, which proves the assumption that current lockdown policies show significant impact on transportation restriction, further reduce vehicle emissions and daily NO<sub>2</sub> concentrations to some extent. These observed-predicted NO<sub>2</sub> differences are considered as baselines to quantify the overall NO<sub>2</sub> variation in each air station.

Figure 4 shows the time-series NO<sub>2</sub> variations values before and during lockdowns in China. The NO<sub>2</sub> variations during lockdowns are within the range of 205 to 3228, which are much higher than those before lockdowns with variation from 46 to 587. This reveals that emissions caused by urban mobility show less impact during lockdowns, leading to greater NO<sub>2</sub> variations compared with the period before lockdown. From the perspective of spatial variation, before lockdowns are proposed, most of the air stations with higher NO<sub>2</sub> variations are located in the eastern and northeastern China, whereas air stations in the southwestern China represent lower differences

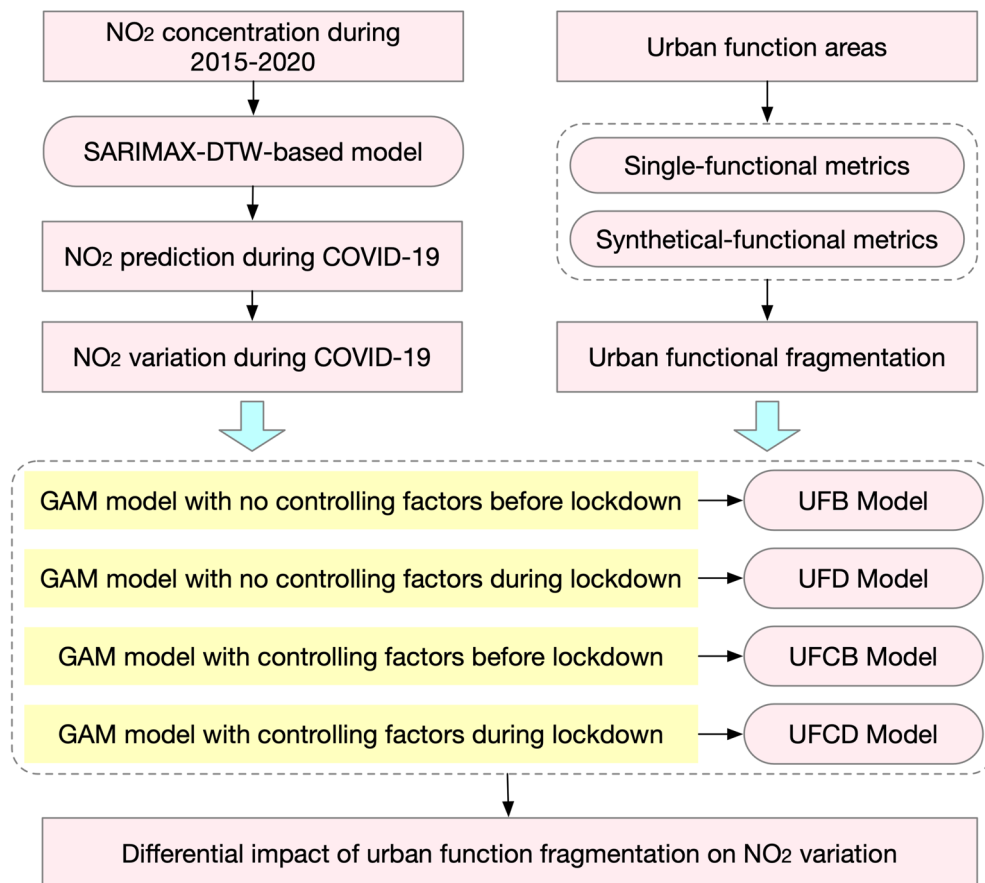


**Figure 1.** The overview framework. Three components are involved, SARIMAX-DTW-based model for NO<sub>2</sub> variation estimation, human-activity-driven urban functional fragmentation quantification and UFB, UFD, UFCB and UFCD Models for association analysis.

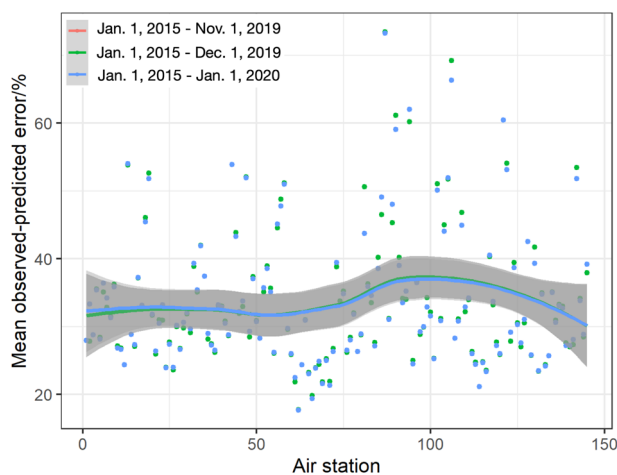


**Figure 2.** Mean daily observed-predicted NO<sub>2</sub> errors based on training data from three time periods, including Jan. 1st, 2015 to Nov. 1st, 2019, from Jan. 1st, 2015 to Dec. 1st, 2019 and from Jan. 1st, 2015 to Jan. 1st, 2020, to determine the time period of training data for SARIMAX modelling.

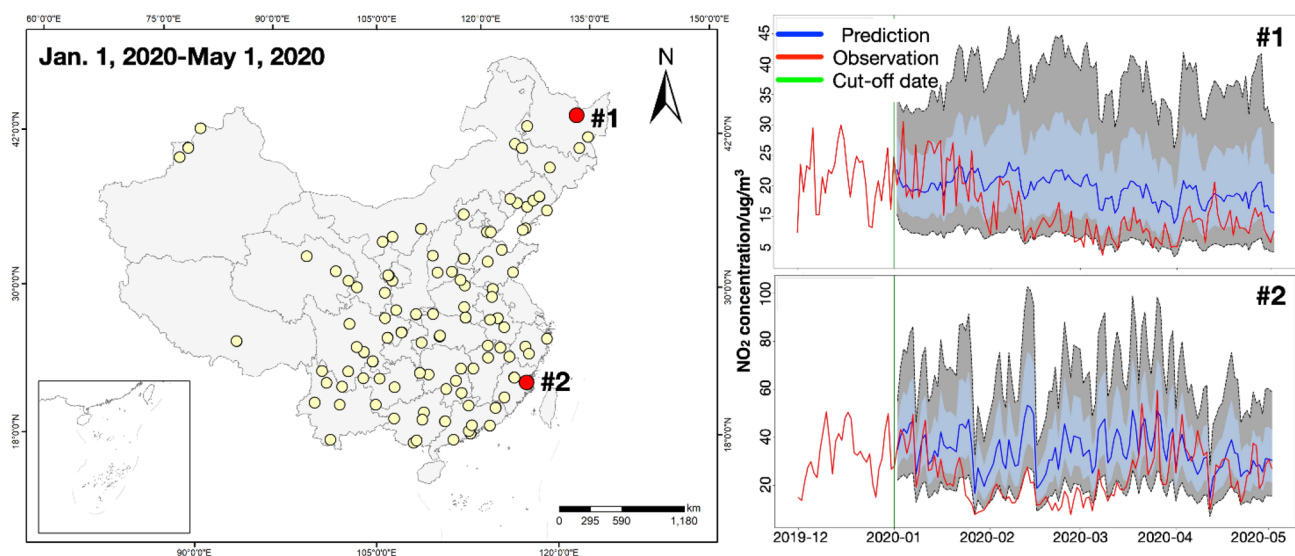


**Figure 3.** Predicted  $\text{NO}_2$  concentrations of selected air stations using SARIMAX during Jan. 1st, 2020 to May 1st, 2020. Two air stations #1 and #2 were selected. Red lines indicate the observed  $\text{NO}_2$  concentrations, blue lines indicate the predicted  $\text{NO}_2$  concentrations, and green lines represent the cut-off date of  $\text{NO}_2$  estimation. The blue and grey areas indicate the one and two standard deviation(s) of  $\text{NO}_2$  predictions. The map is performed using ArcGIS Pro software (version 2.7, <https://www.esri.com/en-us/arcgis/products/arcgis-pro/overview>).

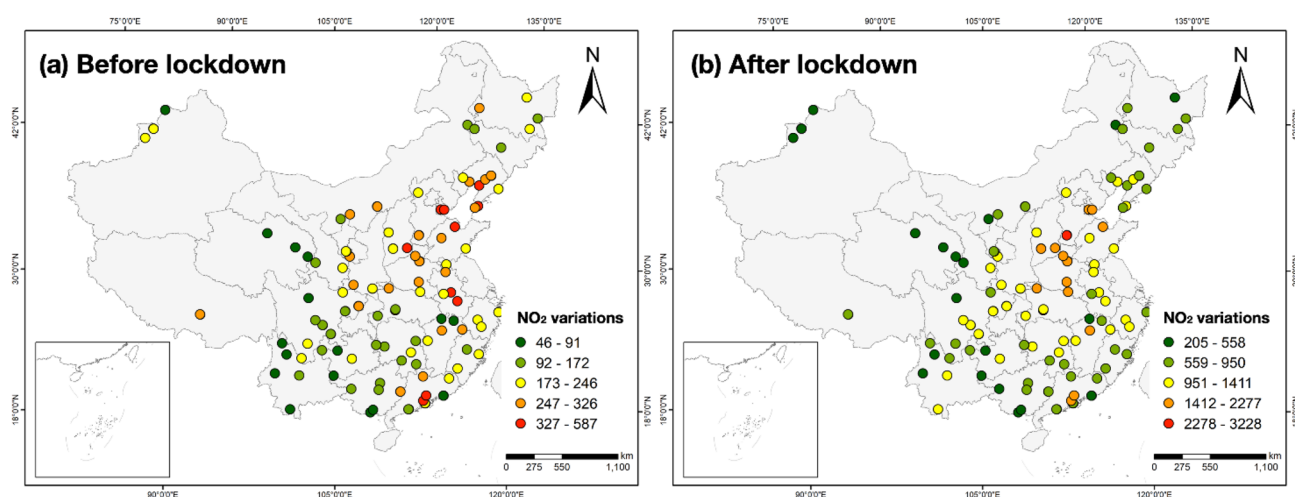


**Figure 4.** Time-series  $\text{NO}_2$  variations between observed and predicted  $\text{NO}_2$  of 145 air stations before and during lockdown calculated using DTW. (a)  $\text{NO}_2$  variations before lockdown; (b)  $\text{NO}_2$  variations during lockdown. High values of  $\text{NO}_2$  variations represent greater changes among observed and predicted  $\text{NO}_2$ . The maps are performed using ArcGIS Pro software (version 2.7, <https://www.esri.com/en-us/arcgis/products/arcgis-pro/overview>).

between observed and predicted  $\text{NO}_2$  concentrations (Fig. 4a). During the lockdowns, the spatial distribution of  $\text{NO}_2$  variations has changed significantly. Specifically, air stations with higher  $\text{NO}_2$  variations mainly distribute in the central east of China, while  $\text{NO}_2$  variation values of the air stations in the north, south and west of China are much lower (Fig. 4b). The detailed quantification of time-series  $\text{NO}_2$  variation is shown in Table S1.

**Urban functional fragmentation.** Based on the extracted 3 km-radius areas among 145 air stations, the spatial variations of the proposed six urban functional fragmentation characteristics were shown in Fig. 5. The edge densities of industrial function among air stations vary from 0.16 to 61.75. Most of the air stations with higher ED values are located in the southern, eastern and central-north China, while air stations with the lowest ED values distribute in the central-south China (Fig. 5a). The spatial distributions of public-functional ED are much different, with higher values observed in the north and southeast coastal areas of China and lower values

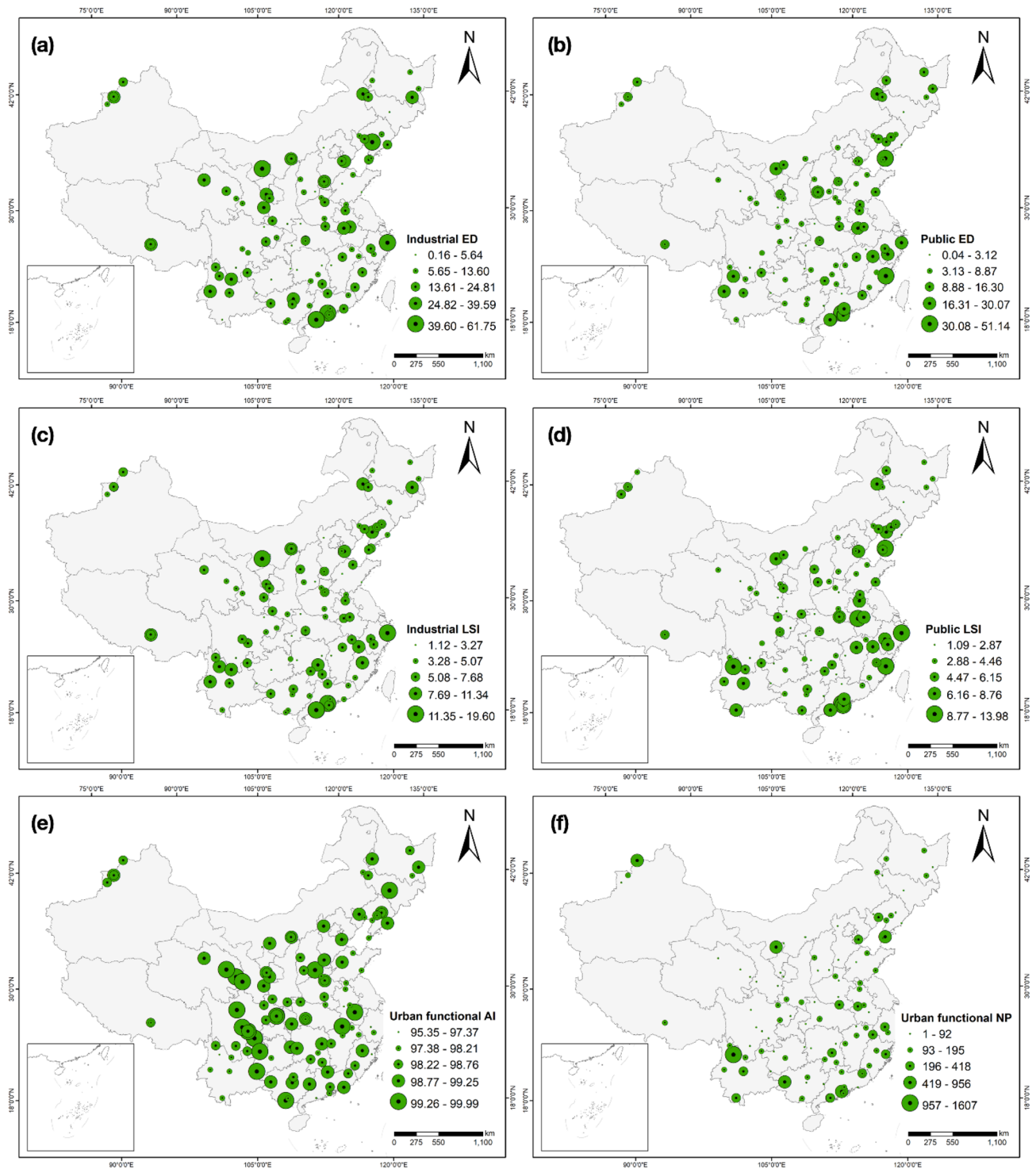


**Figure 5.** Urban functional fragmentation of each air station. (a) Industrial ED; (b) Public ED; (c) Industrial LSI; (d) Public LSI; (e) Urban functional AI; (f) Urban functional NP. The maps are performed using ArcGIS Pro software (version 2.7, <https://www.esri.com/en-us/arcgis/products/arcgis-pro/overview>).

in western and central regions (Fig. 5b). For the depicted industrial LSI, air stations denoting significant higher values are located in the southeastern China, while high-industrial LSI-stations distribute in central and north-west China (Fig. 5c). The spatial pattern of public-functional LSI is similar to the public ED characteristic, with higher degree of complexities distributing in eastern and southwestern China (Fig. 5d). Quantified AI of overall urban functions vary from 95.35 to 99.99, with higher values observed in most of the air stations (Fig. 5e). Spatial patterns of urban functional NP are much different compared with urban functional AI, with solely several

	$R^2$	Deviance explained
UFB Model	0.0807	11.9%
UFD Model	0.107	14.4%
UFCB Model	0.565	64.3%
UFCD Model	0.72	77.4%

**Table 1.** Model evaluation.  $R^2$  values of 0.0807, 0.107, 0.565 and 0.72 and deviance explained percentages of 11.9%, 14.4%, 64.3% and 77.4% of UFB, UFD, UFCB and UFCD Models are revealed. Values of  $R^2$  and deviance explained percentages of UFCB and UFCD Models are much higher than those of UFB and UFD Models.

stations with higher NP values locating sparsely across China (Fig. 5f). The detailed quantification of urban functional fragmentation of 145 air stations is shown in Table S2.

**Effect analysis.** Before the regression models were proposed, the multicollinearity among variables should be tested. In particular, the Variance Inflation Factor (VIF) was utilized to estimate the multicollinearity of urban functional fragmentation variables. The results of VIF values are all lower than 10, indicating that multicollinearity is not high among the variables in the proposed models. On this basis, four regression models were proposed to analyze the effect of urban functional fragmentation on  $\text{NO}_2$  variation, including UFB Model without controlling variables before lockdowns, UFD Model without controlling variables during lockdowns, UFCB Model with controlling variables before lockdowns and UFCD Model with controlling variables during lockdowns. The quantification of  $\text{NO}_2$  variation, urban functional fragmentation and the controlling variables for association analysis is shown in Table S1, S2 and S3, respectively. The results of model evaluation are displayed in Table 1, indicating that involving controlling variables, including population, Air Quality Index (AQI), fine particulate matter with a diameter less than  $2.5 \mu\text{m}$  ( $\text{PM}_{2.5}$ ), particulate matter with a diameter of less than  $10 \mu\text{m}$  ( $\text{PM}_{10}$ ), ozone ( $\text{O}_3$ ), sulfur dioxide ( $\text{SO}_2$ ), carbon monoxide (CO), temperature, humidity and wind speed, is effective to depict  $\text{NO}_2$  variation influenced by urban functional fragmentation with higher accuracies. Moreover, accuracies of UFCD Model during lockdowns are higher than UFCB Model before lockdowns, with 0.565 and 0.72 respectively, indicating that more significant impacts of urban functional fragmentation are shown on  $\text{NO}_2$  variations with restricted anthropogenic emissions compared with the impacts with no emission restrictions. In addition, due to the lower accuracies of UFB Model and UFD model, with 0.0807 and 0.107, the influence of lockdown based on models without controlling variables is insignificant.

The impact of urban functional fragmentation was quantified by the 95%-Confidence-Interval (CI) coefficient changes of the UFB, UFD, UFCB and UFCD models, as shown Fig. 6. Due to the higher accuracy of UFCD, the association between urban functional fragmentation and  $\text{NO}_2$  variations was analyzed with controlling variables and lockdown restrictions. Specifically, the decreasing  $\text{NO}_2$  variations, representing the lower-level  $\text{NO}_2$  differential between COVID-19 lockdowns and normal days, are associated with the increasing industrial ED, public LSI, urban functional AI and NP. The lower-level  $\text{NO}_2$  differential indicates the anthropogenic emissions in fragmented industrial and public lands after lockdown. The synthetical urban functional fragmentations also contribute to the  $\text{NO}_2$  emissions despite of the lockdown and social-distancing restriction. The  $\text{NO}_2$  emission during the lockdown can be explained by the energy uses of the factories in industrial land and essential human activities in public land high-mixing urban functions. On the other hand, increasing  $\text{NO}_2$  variations, representing higher-level  $\text{NO}_2$  differential between COVID-19 lockdowns and normal days, are associated with higher values of public ED and industrial LSI. Based on the declining trends of  $\text{NO}_2$  concentrations in COVID-19 lockdowns which are both found in the previous research<sup>16</sup> and represented in Fig. 3, the  $\text{NO}_2$  differential indicates that the  $\text{NO}_2$  concentrations in lockdowns are much larger than that in normal days. The  $\text{NO}_2$  variation-fragmentation association may due to the reason that higher of public ED and industrial LSI are usually related to large occupation of the green land and small manufacturers with lower energy use.

One should be noted that compared with the major influence of air pollutants and meteorological conditions, only partial impacts of the urban functional fragmentation are revealed. It has been proved by the findings that the accuracies of UFCB and UFCD models are 0.484 and 0.613 higher than UFB and UFD models, respectively. In addition, among all urban functional fragmentation metrics, the highest absolute values of coefficients are attributed by the urban functional AI metric, approximately from 0 to 0.4, while the lowest absolute values of coefficients are revealed in the urban functional NP, approximately from  $5\text{e-}04$  to  $1\text{e-}03$ . The discrepancy of the coefficient ranges may be influenced by the different scale among urban functional fragmentation metrics, in which urban functional AI and NP range from 95.35 to 99.99 and from 1–1067, respectively. Despite of the overall lower coefficients and the diverse coefficients among fragmentation metrics, this study retrieved the partial effect of urban functional fragmentation characteristics by controlling the dominant impact of air pollutants and meteorological factors. Findings could provide suggestions for the government to assess the current urban function planning in  $\text{NO}_2$  controlling.

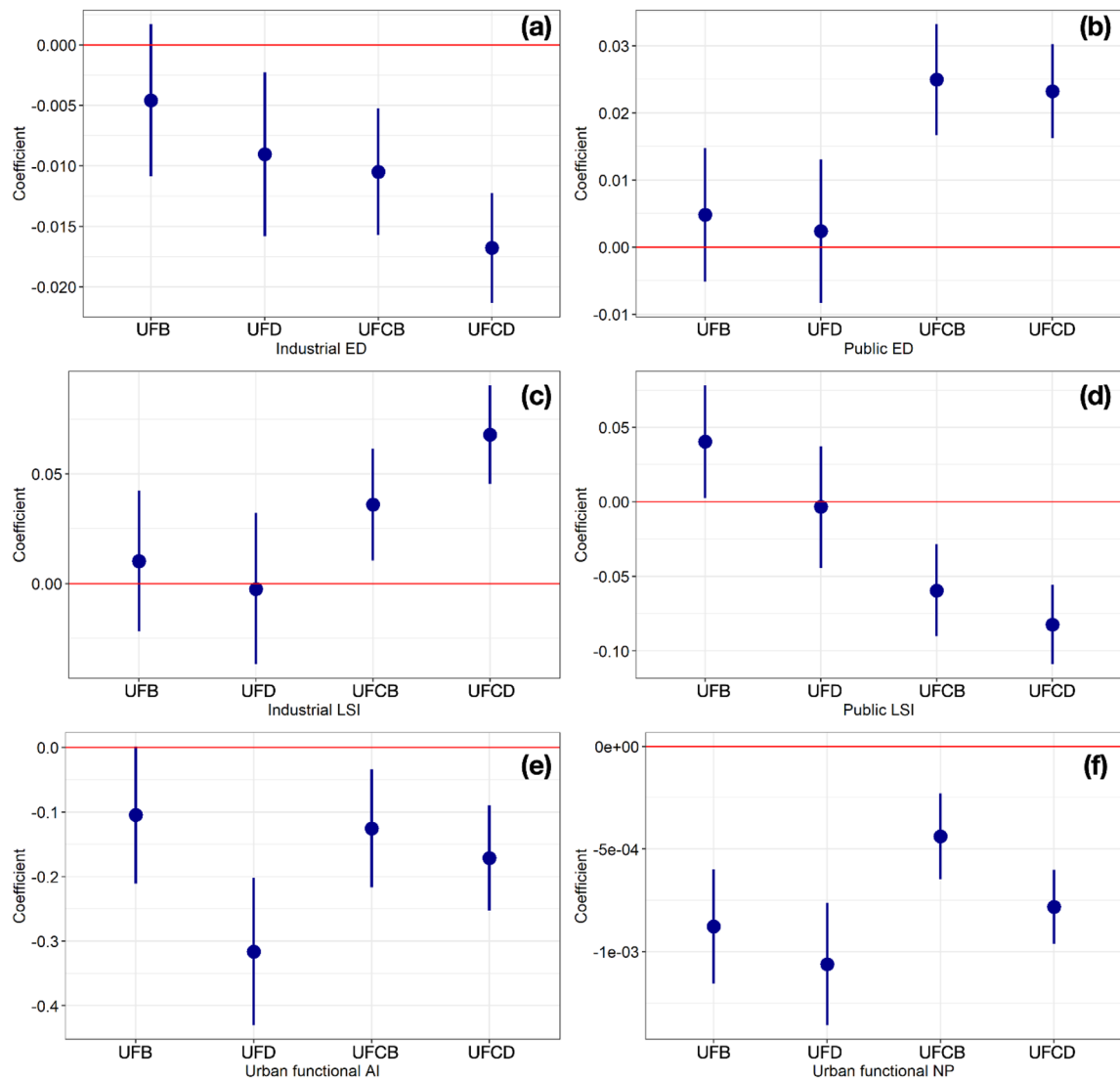


**Figure 6.** Coefficient changes and 95% CI of urban functional fragmentation characteristics on  $\text{NO}_2$  variations based on four models. **(a)** Industrial ED; **(b)** Public ED; **(c)** Industrial LSI; **(d)** Public LSI; **(e)** Urban functional AI; **(f)** Urban functional NP. One unit of industrial ED is associated with  $-0.0046$  (95% CI  $-0.0109$  to  $0.0017$ ),  $-0.0090$  (95% CI  $-0.0158$  to  $-0.0023$ ),  $-0.0105$  (95% CI  $-0.0157$  to  $-0.0053$ ) and  $-0.0168$  (95% CI  $-0.0213$  to  $-0.0122$ )  $\text{NO}_2$  variations of UFB, UFD, UFCB and UFCD models, respectively. Per unit of public ED is linked with  $0.0048$  (95% CI  $-0.0052$  to  $0.0148$ ),  $0.0024$  (95% CI  $-0.0083$  to  $0.0131$ ),  $0.0249$  (95% CI  $0.0166$  to  $0.0332$ ) and  $0.0232$  (95% CI  $0.0162$  to  $0.0303$ )  $\text{NO}_2$  variations for four models.  $\text{NO}_2$  variations of  $0.0103$  (95% CI  $-0.0218$  to  $0.0424$ ),  $-0.0024$  (95% CI  $-0.0370$  to  $0.0321$ ),  $0.0360$  (95% CI  $0.0105$  to  $0.0616$ ) and  $0.0680$  (95% CI  $0.0454$  to  $0.0907$ ) of four models are influenced by per unit of industrial LSI. For the public LSI characteristic, one unit of this is associated with  $0.0405$  (95% CI  $0.0026$  to  $0.0784$ ),  $-0.0035$  (95% CI  $-0.0443$  to  $0.0373$ ),  $-0.0594$  (95% CI  $-0.0902$  to  $-0.0287$ ) and  $-0.0825$  (95% CI  $-0.1092$  to  $-0.0558$ )  $\text{NO}_2$  variations of four models. Per unit of urban functional AI is associated with  $-0.1047$  (95% CI  $-0.2110$  to  $0.0016$ ),  $-0.3165$  (95% CI  $-0.4308$  to  $-0.2022$ ),  $-0.1253$  (95% CI  $-0.2167$  to  $-0.0338$ ) and  $-0.1712$  (95% CI  $-0.2524$  to  $-0.0899$ )  $\text{NO}_2$  variations of four models. One unit of urban functional NP is associated with  $-0.0009$  (95% CI  $-0.0012$  to  $-0.0006$ ),  $-0.0011$  (95% CI  $-0.0014$  to  $-0.0008$ ),  $-0.0004$  (95% CI  $-0.0006$  to  $-0.0002$ ) and  $-0.0008$  (95% CI  $-0.0010$  to  $-0.0006$ )  $\text{NO}_2$  variation of four models.

## Discussion

Based on the coefficient comparison between UFCB Model and UFCD Model (Fig. 6), this section discusses the mediated impacts of anthropogenic air pollutant emissions on the urban functional fragmentation- $\text{NO}_2$  concentration association. As the  $R^2$  values of UFCB and UFCD models with controlling variables are 0.484 and 0.613 higher than UFB and UFD without controlling variables, only UFCB and UFCD models are considered to discuss these mediated impacts. Specifically, the absolute values of coefficients in industrial ED, industrial LSI,

public LSI, urban functional AI and urban functional NP are higher than those in the UFCB Model. The higher absolute values of coefficients in the UFCB Model indicate that greater associations are revealed between urban functional fragmentation and NO<sub>2</sub> variation under the circumstance of anthropogenic-emission restriction. On the other hand, the absolute values of coefficients in public ED in the UFCB Model are lower than those of UFCB Model, which indicates lower association between public ED and NO<sub>2</sub> variations with the effect of anthropogenic-emission restriction. However, the differences of coefficients between UFCB Model and UFCB Model are all lower than 0.1, which indicates the relative limited impact of anthropogenic-emission restriction. Since the changes of NO<sub>2</sub> concentration are significantly influenced by the air pollutant and the meteorological factors and solely partially affected by the urban functional fragmentation, the coefficient changes lower than 0.1 are acceptable to evaluate the mediated impact of anthropogenic-emission restriction.

The findings indicate that based on the anthropogenic-emission restriction, greater impacts of industrial, public and synthetic urban functional fragmentation are shown on the NO<sub>2</sub> variations between COVID-19 and normal days. The greater NO<sub>2</sub> variations during the anthropogenic-emission restrictions can be explained that emissions from the transportation and commercial functions have been significantly reduced due to the lockdown and social-distancing restriction. In addition, the directions (namely positive or negative trends) of urban functional fragmentation-NO<sub>2</sub> variation association are not changed by the mediated impact of the anthropogenic-emission restriction.

This study provides an insight into evaluating urban functional fragmentation patterns that are associated with NO<sub>2</sub> emissions under the circumstance of COVID-19 lockdowns, which could support managers and policymakers to allocate urban resources and public facilities. Specifically, assessing the spatial distribution of industrial and public functions in terms of the degree of fragmentation can be useful for implementing a sustainable environment development strategy. While the influence of transportation on air quality has been restricted during COVID-19 lockdowns, energy uses associated with the heterogeneous expanding of industrial and public lands should be concerned. This study has also provided suggestions for the governments which specific fragmentation characteristics can be concerned in a higher priority. For instance, we have found that fragmentation patterns of public LSI show the higher potential to contribute to NO<sub>2</sub> emissions compared with the public ED.

The government should also be sensitive to the synthetic influence of urban functions and the corresponding fragmentation patterns. The increasing number and aggregation degree of urban function patches may contribute to the demands of accessibility to different public facilities, rendering the potential factors to increase anthropogenic air pollution emissions. Despite that the complexity urban structures and functions can improve urban vitality and socioeconomic development, the negative effect on air quality should be concerned to mitigate public health risk. Accordingly, the governments should keep the balance between urban vitality and air quality caused by urban functional fragmentations to develop sustainable societies.

## Conclusion

This study explored the impact of urban functional fragmentation on NO<sub>2</sub> variations with anthropogenic-emission restriction in China. Counterfactual NO<sub>2</sub> concentrations during COVID-19 were predicted based on historical NO<sub>2</sub> patterns using SARIMAX and were further utilized to quantify the variations comparing with the NO<sub>2</sub> in normal days using DTW. Then, characteristics including industrial/public ED and LSI and urban functional AI and NP were utilized to depict urban functional fragmentation. Four models, including UFB, UFD, UFCB and UFCB Models based on GAMs are further proposed to investigate the impact of urban functional fragmentations on NO<sub>2</sub> variations before and during COVID-19 lockdowns.

The results reveal that under the circumstance of anthropogenic-emission restriction, industrial ED, public LSI, urban functional AI and NP are negatively associated with NO<sub>2</sub> variations, while public ED and industrial LSI are positively related to NO<sub>2</sub> variations. Compared with the fragmentation-NO<sub>2</sub> variation association before lockdown, the mediated impact of anthropogenic-emission restriction partially increases the effect of industrial ED, industrial LSI, public LSI, urban functional AI and urban functional NP while decreases the effect of public ED on NO<sub>2</sub> variation, with the absolute values of coefficients ranging within 0.1. However, the impact of restricted anthropogenic emissions does not change the positive or negative directions of fragmentation-NO<sub>2</sub> variation association.

Although the proposed research has explored the urban functional fragmentation patterns associated with NO<sub>2</sub> variation, limitations still exist and are required to be solved in future studies. In quantifying NO<sub>2</sub> variation, the variations between observed and predicted NO<sub>2</sub> concentrations are measured. Although the performance of SARIXAM has been evaluated by comparing forecasting results in different time periods, the prediction errors during COVID-19 lockdown cannot be eliminated. As a result, the coefficients of NO<sub>2</sub> variations could be influenced by these errors. To avoid this issue, regression model will be modified by concerning forecasting biases as controlling variables in further research. Moreover, as only fragmentation characteristics are involved in depicting urban functional morphologies, the spatial heterogeneity and also its dynamics of different functions should also be involved in future studies. In addition, only the potential impact of urban functional fragmentation on NO<sub>2</sub> variation has been investigated. How to integrate the fragmentation factors with human activities based on the restricted anthropogenic emissions to predict the on-going NO<sub>2</sub> variation remain an issue to be solved.

## Methods

**Data sources.** Daily surface NO<sub>2</sub> observations from the China National Environmental Monitoring Center (CNEMC) (available at <http://106.37.208.233:20035/>) were adopted. Considering of the temporal changes of long-term NO<sub>2</sub>, daily surface NO<sub>2</sub> from Jan. 1st, 2015 to May 1st, 2020 were collected<sup>51</sup>. Specifically, a total number of 145 sites were involved, occupying 27 provinces throughout mainland China. In addition, controlling variables, including population, AQI, PM<sub>2.5</sub>, PM<sub>10</sub>, O<sub>3</sub>, SO<sub>2</sub>, CO, temperature, humidity and wind speed, are

also collected. In particular, AQI, PM<sub>2.5</sub>, PM<sub>10</sub>, O<sub>3</sub>, SO<sub>2</sub>, and CO are collected from CNEMC, while temperature, humidity and wind speed are collected in the weather stations from the China National Meteorological Science Data Center (CMA) (available at <https://data.cma.cn>). It should be noted that as NO<sub>2</sub> sites and weather stations usually are not located in the same location, weather stations which are nearest to the NO<sub>2</sub> sites are chosen to quantify the corresponding meteorological data.

For the data source utilized to depict urban functional fragmentation, urban function classification is adopted from urban land use category mapping proposed by Gong, et al.<sup>52</sup>. In particular, level-1 land use classification scheme was utilized, including residential, commercial, industrial, transportation and public management and service, to represent corresponding urban functions.

**Estimation of NO<sub>2</sub> variation.** NO<sub>2</sub> varies drastically during the lockdowns in COVID-19 because of the restricted urban mobility. In particular, the variation of NO<sub>2</sub> concentrations can be quantified based on the differences of NO<sub>2</sub> in lockdowns and NO<sub>2</sub> in normal days. While NO<sub>2</sub> concentrations in lockdowns are observed through air stations, NO<sub>2</sub> concentrations in normal days can be predicted according to the periodical patterns of historical NO<sub>2</sub> concentrations. A SARIMAX-DTW-based model is proposed to quantify NO<sub>2</sub> variations in this study. Specifically, counterfactual NO<sub>2</sub> concentrations during COVID-19 (from Jan. 1st, 2020 to May 1st, 2020) are predicted based on historical NO<sub>2</sub> using SARIMAX model, with exogenous variables including air temperature, relative humidity and wind speed. The basic SARIMAX model can be presented as follows:

$$\text{SARIMAX}(p, d, q)(P, D, Q)_t \quad (1)$$

in which  $p, d, q$  denote the autoregressive order, difference order and moving average order, while  $P, D, Q$  indicate the seasonal autoregressive order, difference order and moving average order, respectively. To determine those parameters, the Augmented Dickey-Fuller test and Osborn, Chui, Smith, and Birchenhall test and Canova-Hansen test. In addition, the Ljung-Box test and the Jarque-Bera test are applied to examine the randomness and normality of the time series. The performances of SARIMAX with different parameters are evaluated by Akaike Information Criterion (AIC).

As this study aims on predicting the temporal patterns of NO<sub>2</sub> during COVID-19 using SARIMAX, under the assumption that no lockdown policies are proposed, historical NO<sub>2</sub> concentrations are required for model training. In particular, NO<sub>2</sub> from three different time periods before COVID-19 epidemic are utilized as training data, including NO<sub>2</sub> (1) from Jan. 1st, 2015 to Nov. 1st, 2019, (2) from Jan. 1st, 2015 to Dec. 1st, 2019 and (3) from Jan. 1st, 2015 to Jan. 1st, 2020. And the corresponding data for NO<sub>2</sub> prediction in normal days includes NO<sub>2</sub> (1) from Nov. 1st, 2019 to May 1st, 2020, (2) from Dec. 1st, 2019 to May 1st, 2020, and from (3) Jan. 1st, 2020 to May 1st, 2020. Because of the time inconsistency of COVID-19 outbreaks in different regions in China, the model accuracies are evaluated based on different time period division. Furthermore, to evaluate the proposed SARIMAX models with different time periods, mean observed-predicted NO<sub>2</sub> errors for each air station are calculated:

$$\text{MOPE}_i = \sum_{k=1}^n \frac{|NO_{2obs,k} - NO_{2pre,k}|}{NO_{2obs,k}} / n \cdot 100 \quad (2)$$

where  $\text{MOPE}_i$  refers to the mean daily observed-predicted NO<sub>2</sub> error of the  $i$ th air station.  $NO_{2obs,k}$  and  $NO_{2pre,k}$  represent the observed NO<sub>2</sub> concentrations and the predicted NO<sub>2</sub> concentrations of the  $k$ th day, respectively.  $n$  is the total number of days during time periods. Specifically, time period with lower values of  $\text{MOPE}_i$  is selected for SARIMAX modelling.

To investigate the effects of restricted urban mobility during COVID-19, variations between the actual and counterfactual NO<sub>2</sub> concentrations are required to be quantified. Moreover, NO<sub>2</sub> variation should be matched with optional alignment instead of day-to-day matching to reduce prediction errors of SARIMAX model. Thus, the DTW model is utilized to fit the non-linear patterns of NO<sub>2</sub> concentrations. NO<sub>2</sub> variation between the actual and counterfactual time periods are calculated as follows:

$$\text{DTW}(T_{act}, T_{cou}) = \arg \min_{W=w_1 \dots w_K \dots w_K} \sqrt{\sum_{k=1, w_k=(i,j)}^K (t_{act,i} - t_{con,j})^2} \quad (3)$$

where  $T_{act}$  and  $T_{con}$  refer to the actual and counterfactual temporal NO<sub>2</sub> concentrations during COVID-19 epidemic.  $W$  represents the warping path aligned by  $T_{act}$  and  $T_{con}$ . Higher  $\text{DTW}(T_{act}, T_{con})$  values denote higher degree of NO<sub>2</sub> variation.

**Urban functional fragmentation metrics.** This study measures urban functional fragmentation from two perspectives, including single-urban functional fragmentation and overall urban functional fragmentation, as shown in Table 2. For the single-urban functional fragmentation, industrial and public functions are considered as they are highly associated with anthropogenic air pollutant emissions<sup>33,34</sup>. In particular, as the urbanization process may change the monotonous patterns to heterogenous distribution such as the emerging of small areas of parks and hospitals, the complexities of industrial and public function patches can effectively exhibit varying trends of anthropogenic energy uses (such as the increasing transportation). Research has

	Indicator	Equation	Definition	Fragmentation application
Single-urban functional fragmentation depiction	Industrial/Public Edge Density (ED)	$ED = \frac{\sum_{k=1}^m e_{ik}}{A}$	$e_{ik}$ indicates the total length of edge of a certain patch $k$ belonging to the $i$ th class. $m$ indicates the total number of patches of the $i$ th class. $A$ refers to the total areas belonging to the $i$ th urban functional class	As most of the anthropogenic emissions are generated from industrial and public lands, the shape complexities depicted by ED and LSI of industrial and public urban functional patches are considered. Higher values of ED and LSI indicate higher degree of edge density and complexity, respectively
	Industrial/Public Landscape Shape Index (LSI)	$LSI = \frac{0.25 \sum_{k=1}^m e_{ik}}{\sqrt{A}}$		
Synthetical urban functional fragmentation depiction	Urban functional Aggregation Index (AI)	$AI = \left[ \sum_{i=1}^m \left( \frac{g_{ii}}{\max(g_{ii})} \right) P_i \right] \cdot (100)$	$g_{ii}$ represent the number of like adjacencies between pixels of the patches of the $i$ th class. $\max(g_{ii})$ refers to the maximum number of $g_{ii}$ . $P_i$ denotes the percentage of the $i$ th urban functional class within each 3 km-radius area. $N$ refers to the total number of urban functional patches within individual buffers	For all-type urban functions, higher values of NP represent large total number of urban functional patches and higher fragmentation degree within individual buffers. The AI values increase as the urban functional patches within buffers are increasingly aggregated
	Urban functional Number of Patches (NP)	$NP = N$		

**Table 2.** Indicators for depicting urban functional fragmentation.

revealed the potential relationship between impervious LSI and the edge characteristics of public spaces and  $\text{NO}_2$  distribution<sup>22,53</sup>. This study adopts metrics including industrial/public ED and LSI to depict the fragmentation characteristics in terms of patch complexity.

For the overall urban functional fragmentation, the changes of the regular patterns of human activities (such as the synthetic influence of manufacturing, residential and transportation) that lead to the anthropogenic-emission variation are considered. To depict these specific fragmentation characteristics, the possible increased number of urban function patches and their connections are utilized. Liang, et al.<sup>54</sup> have discussed the effect of AI landscape characteristics of urban forms on  $\text{NO}_2$  concentrations, while characteristics of patch number and density in metropolitan regions have been evaluated with the influence on air quality<sup>55</sup>. Thus, this study adopts AI and NP metrics for quantifying synthetic urban functional patterns.

To depict urban functional fragmentation characteristics based on the proposed metrics, continuous areas around air station are extracted as station-sensed regions. In particular, the buffer of each air station within 3 km is chosen, as previous studies have revealed that radius of air stations within approximately 2.5 km are highly correlated with  $\text{NO}_2$  concentrations<sup>56,57</sup>. On this basis, 3 km-radius areas of 145 air stations were extracted. Among the 145 air stations, 27 air stations were randomly chosen for displaying the urban function distributions. As shown in Fig. 7, the proportions of urban functional occupation vary among different cities.

**Statistical analysis.** The effects of urban functional fragmentation on  $\text{NO}_2$  variation before and during lockdowns (lockdown date is selected as Jan. 24, 2020) during COVID-19 are analyzed using GAMs. Specifically, the proposed GAMs are implemented based on Gaussian distribution.  $\text{NO}_2$  variation are utilized as dependent variable while six urban functional fragmentation characteristics, including industrial ED, public ED, industrial LSI, public LSI, urban functional AI and urban functional NP, are considered as independent variables. In addition, possible confounding effects, including population, AQI,  $\text{PM}_{2.5}$ ,  $\text{PM}_{10}$ ,  $\text{O}_3$ ,  $\text{SO}_2$ , CO, temperature, humidity and wind speed, are involved as controlling variables. The average daily values of AQI,  $\text{PM}_{2.5}$ ,  $\text{PM}_{10}$ ,  $\text{O}_3$ ,  $\text{SO}_2$ , CO, temperature, humidity and wind speed are adopted while the total population within the 3-km buffers around the air stations is utilized. Then, four comparative models are designed, concerning additional environmental factor for model controlling and different scenarios, namely before and during COVID-19 lockdown<sup>16,58</sup> (Table 3): (1) UFB Model, including urban functional fragmentation characteristics before lockdowns; (2) UFD Model, including urban functional fragmentation characteristics during lockdowns; (3) UFCB Model, including both urban functional fragmentation characteristics and controlling variables before lockdowns; and (4) UFCD Model, including urban functional fragmentation characteristics and controlling variables during lockdowns. The proposal GAMs in UFB Model and UFD Model are defined as Eq. (4) and GAMs in UFCB Model and UFCD Model are defined as Eq. (5), respectively:

$$\log E(Y_i) = \alpha + \beta_1 \text{Ind}_{EDi} + \beta_2 \text{Pub}_{EDi} + \beta_3 \text{Ind}_{LSIi} + \beta_4 \text{Pub}_{LSIi} + \beta_5 \text{UF}_{Ai} + \beta_6 \text{UF}_{NPi} \quad (4)$$

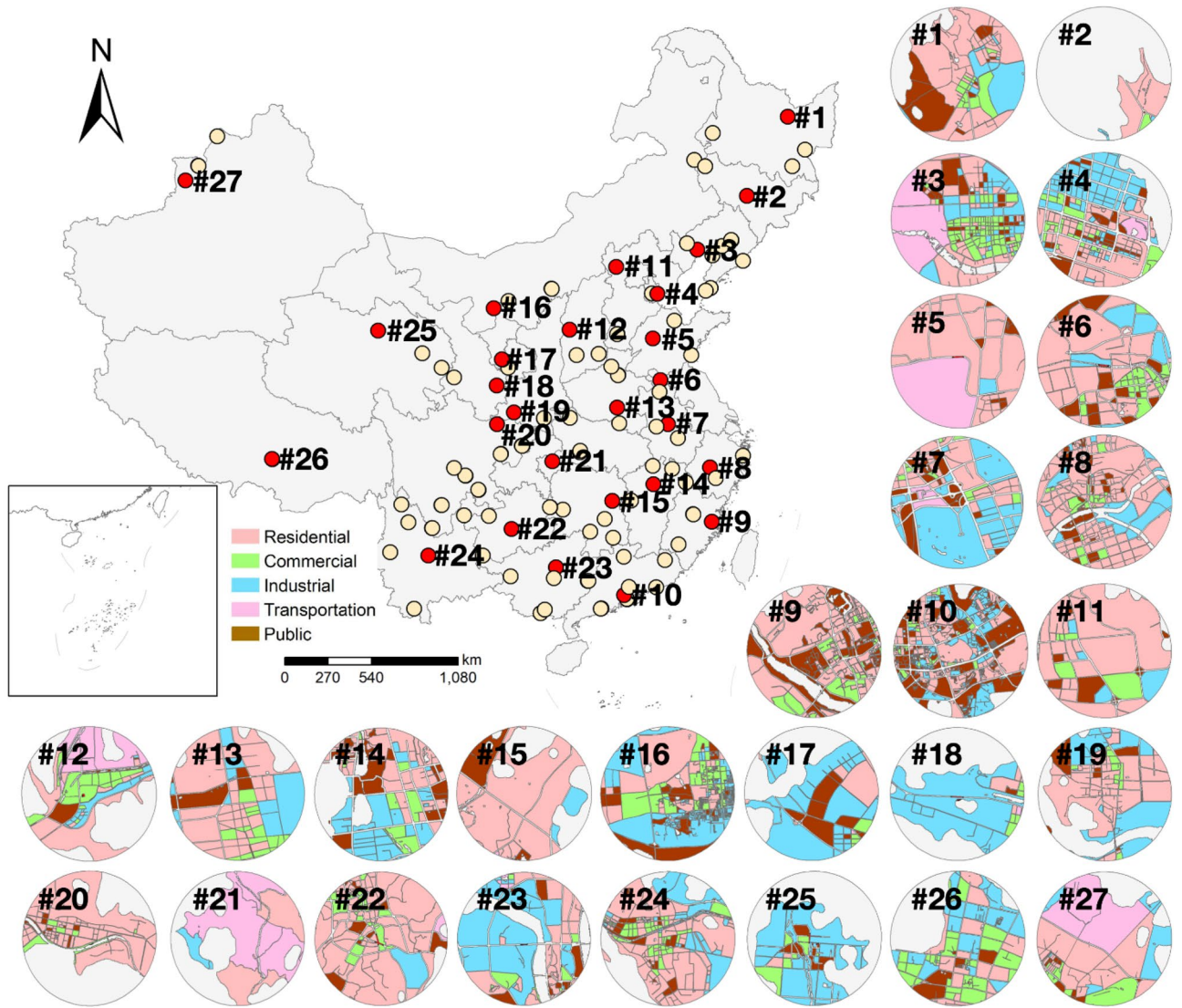


**Figure 7.** Distribution of urban functions within buffers of selected air stations. 27 sites of 145 air stations with 3 km buffers were displayed. Urban functions including residential, commercial, industrial, transportation and public functions are involved to depict fragmentation characteristics. The maps are performed using ArcGIS Pro software (version 2.7, <https://www.esri.com/en-us/arcgis/products/arcgis-pro/overview>).

$$\begin{aligned}
 \log E(Y_i) = & \alpha + \beta_1 Ind_{ED_i} + \beta_2 Pub_{ED_i} + \beta_3 Ind_{LSI_i} + \beta_4 Pub_{LSI_i} \\
 & + \beta_5 UF_{AI_i} + \beta_6 UF_{NP_i} + s(Pop_i) + s(AQI_i) + s(PM_{2.5_i}) \\
 & + s(PM_{10_i}) + s(O_{3_i}) + s(CO_i) + s(SO_{2_i}) \\
 & + s(Tem_i) + s(Hum_i) + s(Wind_i)
 \end{aligned}
 \tag{5}$$

where  $E(Y_i)$  is the expected  $NO_2$  differences of the  $i$ th air station during COVID-19.  $\alpha$  and  $\beta$  are the intercept and regression coefficient, respectively.  $Ind_{ED_i}$ ,  $Pub_{ED_i}$ ,  $Ind_{LSI_i}$ ,  $Pub_{LSI_i}$ ,  $UF_{AI_i}$  and  $UF_{NP_i}$  are the fragmentation characteristics depicting urban functions including industrial ED, public ED, industrial LSI, public LSI, urban functional AI and urban functional NP of the  $i$ th air station.  $Pop_i$ ,  $AQI_i$ ,  $PM_{2.5_i}$ ,  $PM_{10_i}$ ,  $O_{3_i}$ ,  $SO_{2_i}$ ,  $CO_i$ ,  $Tem_i$ ,  $Hum_i$  and  $Wind_i$  represent the controlling variables including population, AQI,  $PM_{2.5}$ ,  $PM_{10}$ ,  $O_3$ ,  $SO_2$ ,  $CO$ , temperature, humidity and wind speed of the  $i$ th air station, respectively.  $s(variable)$  refers to the smoother function of a specific variable based on the penalized smoothing spline, with the degree of freedom evaluated by Akaike Information Criterion (AIC).

Variables		UFB Model	UFD Model	UFCB Model	UFCD Model
		Before lockdown	During lockdown	Before lockdown	During lockdown
Independent variables	Industrial ED	✓	✓	✓	✓
	Public ED	✓	✓	✓	✓
	Industrial LSI	✓	✓	✓	✓
	Public LSI	✓	✓	✓	✓
	Urban functional AI	✓	✓	✓	✓
	Urban functional NP	✓	✓	✓	✓
Controlling variables	Population			✓	✓
	AQI			✓	✓
	PM <sub>2.5</sub> (μg/m <sup>3</sup> )			✓	✓
	PM <sub>10</sub> (μg/m <sup>3</sup> )			✓	✓
	O <sub>3</sub> (μg/m <sup>3</sup> )			✓	✓
	CO (mg/m <sup>3</sup> )			✓	✓
	SO <sub>2</sub> (μg/m <sup>3</sup> )			✓	✓
	Temperature (°C)			✓	✓
	Humidity (%)			✓	✓
	Wind speed (m/s)			✓	✓
Dependent variables	NO <sub>2</sub> variation	✓	✓	✓	✓

**Table 3.** Independent and dependent variables for GAMs.

Received: 1 January 2021; Accepted: 18 May 2021

Published online: 07 June 2021

## References

- Gbanie, S. P., Griffin, A. L. & Thornton, A. Impacts on the urban environment: Land cover change trajectories and landscape fragmentation in post-war Western Area Sierra Leone. *Remote Sens.* **10**, 129 (2018).
- Sheng, N., Tang, U. W. & Grydehøj, A. Urban morphology and urban fragmentation in Macau, China: island city development in the Pearl River Delta megacity region. *Island Stud. J.* **12**, 199–212 (2017).
- Jaeger, J. A. *et al.* Implementing landscape fragmentation as an indicator in the Swiss Monitoring System of Sustainable Development (MONET). *J. Environ. Manage.* **88**, 737–751 (2008).
- Lee, G.-G., Lee, H.-W. & Lee, J.-H. Greenhouse gas emission reduction effect in the transportation sector by urban agriculture in Seoul Korea. *Landscape Urban Plan.* **140**, 1–7 (2015).
- Clark, C. *et al.* Does traffic-related air pollution explain associations of aircraft and road traffic noise exposure on children's health and cognition? A secondary analysis of the United Kingdom sample from the RANCH project. *Am. J. Epidemiol.* **176**, 327–337 (2012).
- Achakulwisut, P., Brauer, M., Hystad, P. & Anenberg, S. C. Global, national, and urban burdens of paediatric asthma incidence attributable to ambient NO<sub>2</sub> pollution: estimates from global datasets. *Lancet Planetary Health* **3**, e166–e178 (2019).
- Beelen, R. *et al.* Long-term effects of traffic-related air pollution on mortality in a Dutch cohort (NLCS-AIR study). *Environ. Health Perspect.* **116**, 196–202 (2008).
- Filleul, L. *et al.* Twenty five year mortality and air pollution: results from the French PAARC survey. *Occup. Environ. Med.* **62**, 453–460 (2005).
- Volz, A. & Kley, D. Evaluation of the Montsouris series of ozone measurements made in the nineteenth century. *Nature* **332**, 240–242 (1988).
- WHO. *Air quality guidelines: global update 2005: particulate matter, ozone, nitrogen dioxide, and sulfur dioxide.* (World Health Organization, 2006).
- Dutheil, F., Baker, J. S. & Navel, V. COVID-19 as a factor influencing air pollution? *Environmental Pollution (Barking, Essex: 1987)* **263**, 114466 (2020).
- Bherwani, H. *et al.* Understanding COVID-19 transmission through Bayesian probabilistic modeling and GIS-based Voronoi approach: a policy perspective. *Environment, Development and Sustainability*, 1–19 (2020).
- Gautam, S. The influence of COVID-19 on air quality in India: a boon or inutility. *Bull. Environ. Contam. Toxicol.* **104**, 724–726 (2020).
- Gupta, A. *et al.* Air pollution aggravating COVID-19 lethality? Exploration in Asian cities using statistical models. *Environment, Development and Sustainability*, 1–10 (2020).
- Bherwani, H. *et al.* Valuation of air pollution externalities: comparative assessment of economic damage and emission reduction under COVID-19 lockdown. *Air Qual. Atmos. Health* **13**, 683–694 (2020).
- Venter, Z. S., Aunan, K., Chowdhury, S. & Lelieveld, J. COVID-19 lockdowns cause global air pollution declines. *Proc. Natl. Acad. Sci.* **117**, 18984–18990 (2020).
- Cohen, J. & Kupferschmidt, K. (American Association for the Advancement of Science, 2020).
- Shi, K., Di, B., Zhang, K., Feng, C. & Svirchev, L. Detrended cross-correlation analysis of urban traffic congestion and NO<sub>2</sub> concentrations in Chengdu. *Transp. Res. Part D: Transp. Environ.* **61**, 165–173 (2018).
- Gautam, A. S. *et al.* Temporary reduction in air pollution due to anthropogenic activity switch-off during COVID-19 lockdown in northern parts of India. *Environment, Development and Sustainability*, 1–24 (2020).
- Gautam, S. COVID-19: air pollution remains low as people stay at home. *Air Qual. Atmos. Health* **13**, 853–857 (2020).
- Lee, C. Impacts of urban form on air quality in metropolitan areas in the United States. *Comput. Environ. Urban Syst.* **77**, 101362 (2019).
- Song, W., Jia, H., Li, Z., Tang, D. & Wang, C. Detecting urban land-use configuration effects on NO<sub>2</sub> and NO variations using geographically weighted land use regression. *Atmos. Environ.* **197**, 166–176 (2019).

23. Li, C., Wang, Z., Li, B., Peng, Z.-R. & Fu, Q. Investigating the relationship between air pollution variation and urban form. *Build. Environ.* **147**, 559–568 (2019).
24. Xing, H. & Meng, Y. Measuring urban landscapes for urban function classification using spatial metrics. *Ecol. Ind.* **108**, 105722 (2020).
25. Vanderhaegen, S. & Canters, F. Mapping urban form and function at city block level using spatial metrics. *Landsc. Urban Plan.* **167**, 399–409 (2017).
26. Shi, K. *et al.* Effects of urban forms on CO<sub>2</sub> emissions in China from a multi-perspective analysis. *J. Environ. Manage.* **262**, 110300 (2020).
27. Bechle, M. J., Millet, D. B. & Marshall, J. D. Does urban form affect urban NO<sub>2</sub>? Satellite-based evidence for more than 1200 cities. *Environ. Sci. Technol.* **51**, 12707–12716 (2017).
28. Huang, S.-L., Lai, H.-Y. & Lee, C.-L. Energy hierarchy and urban landscape system. *Landsc. Urban Plan.* **53**, 145–161 (2001).
29. Wakefield, S. E., Elliott, S. J., Cole, D. C. & Eyles, J. D. Environmental risk and (re) action: air quality, health, and civic involvement in an urban industrial neighbourhood. *Health Place* **7**, 163–177 (2001).
30. Fan, W., Wang, H., Liu, Y. & Liu, H. Spatio-temporal variation of the coupling relationship between urbanization and air quality: a case study of Shandong Province. *J. Clean. Prod.* **272**, 122812 (2020).
31. He, L., Liu, Y., He, P. & Zhou, H. Relationship between air pollution and urban forms: Evidence from prefecture-level cities of the Yangtze River Basin. *Int. J. Environ. Res. Public Health* **16**, 3459 (2019).
32. Marmett, B., Carvalho, R. B., Rhoden, F. R. & Rhoden, C. R. Seasonal influence in traffic-related air pollutants concentrations in urban parks from Porto Alegre Brazil. *Open J. Air Pollut.* **8**, 96–107 (2019).
33. Xing, Y. & Brimblecombe, P. Role of vegetation in deposition and dispersion of air pollution in urban parks. *Atmos. Environ.* **201**, 73–83 (2019).
34. Lee, C. Impacts of urban form on air quality: Emissions on the road and concentrations in the US metropolitan areas. *J. Environ. Manage.* **246**, 192–202 (2019).
35. Li, F. & Zhou, T. Effects of urban form on air quality in China: An analysis based on the spatial autoregressive model. *Cities* **89**, 130–140 (2019).
36. Liang, L. & Gong, P. Urban and air pollution: a multi-city study of long-term effects of urban landscape patterns on air quality trends. *Sci. Rep.* **10**, 1–13 (2020).
37. Goldberg, D. L. *et al.* Disentangling the impact of the COVID-19 lockdowns on urban NO<sub>2</sub> from natural variability. *Geophysical Research Letters*, e2020GL089269 (2020).
38. Baldasano, J. M. COVID-19 lockdown effects on air quality by NO<sub>2</sub> in the cities of Barcelona and Madrid (Spain). *Science of the Total Environment*, 140353 (2020).
39. Berman, J. D. & Ebisu, K. Changes in US air pollution during the COVID-19 pandemic. *Sci. Total Environ.* **739**, 139864 (2020).
40. Muhammad, S., Long, X. & Salman, M. COVID-19 pandemic and environmental pollution: a blessing in disguise? *Science of the Total Environment*, 138820 (2020).
41. Richter, A., Burrows, J. P., Nüß, H., Granier, C. & Niemeier, U. Increase in tropospheric nitrogen dioxide over China observed from space. *Nature* **437**, 129–132 (2005).
42. Wu, Y., Shan, L., Guo, Z. & Peng, Y. Cultivated land protection policies in China facing 2030: Dynamic balance system versus basic farmland zoning. *Habitat Int.* **69**, 126–138 (2017).
43. Fang, C. & Wen, Z. in *The Chinese Economy 75–90* (Springer, 2012).
44. Tan, M. H., Li, X. B. & Lu, C. H. An analysis of driving forces of urban land expansion in China. *Econ. Geogr.* **5**, 012 (2003).
45. Gong, J., Jiang, C., Chen, W., Chen, X. & Liu, Y. Spatiotemporal dynamics in the cultivated and built-up land of Guangzhou: Insights from zoning. *Habitat Int.* **82**, 104–112 (2018).
46. Liu, X. *et al.* Understanding urban China with open data. *Cities* **47**, 53–61 (2015).
47. Cai, B., Guo, H., Cao, L., Guan, D. & Bai, H. Local strategies for China's carbon mitigation: An investigation of Chinese city-level CO<sub>2</sub> emissions. *J. Clean. Prod.* **178**, 890–902 (2018).
48. Wang, C., Horby, P. W., Hayden, F. G. & Gao, G. F. A novel coronavirus outbreak of global health concern. *Lancet* **395**, 470–473 (2020).
49. Chen, K., Wang, M., Huang, C., Kinney, P. L. & Anastas, P. T. Air pollution reduction and mortality benefit during the COVID-19 outbreak in China. *Lancet Planetary Health* **4**, e210–e212 (2020).
50. He, G., Pan, Y. & Tanaka, T. The short-term impacts of COVID-19 lockdown on urban air pollution in China. *Nature Sustainability*, 1–7 (2020).
51. Zhang, L., Lee, C. S., Zhang, R. & Chen, L. Spatial and temporal evaluation of long term trend (2005–2014) of OMI retrieved NO<sub>2</sub> and SO<sub>2</sub> concentrations in Henan Province. *China Atmos. Environ.* **154**, 151–166 (2017).
52. Gong, P. *et al.* Mapping essential urban land use categories in China (EULUC-China): preliminary results for 2018. *Sci. Bull.* **65**, 182–187 (2020).
53. Jaafari, S., Shabani, A. A., Moeinaddini, M., Danekar, A. & Sakieh, Y. Applying landscape metrics and structural equation modeling to predict the effect of urban green space on air pollution and respiratory mortality in Tehran. *Environ. Monit. Assess.* **192**, 1–15 (2020).
54. Liang, Z. *et al.* The context-dependent effect of urban form on air pollution: a panel data analysis. *Remote Sens.* **12**, 1793 (2020).
55. She, Q. *et al.* Air quality and its response to satellite-derived urban form in the Yangtze River Delta China. *Ecol. Indic.* **75**, 297–306 (2017).
56. Li, C. *et al.* Application of land use regression for estimating concentrations of major outdoor air pollutants in Jinan China. *J. Zhejiang Univ. Sci. A* **11**, 857–867 (2010).
57. Kumar, R. & Joseph, A. E. Air pollution concentrations of PM<sub>25</sub>, PM<sub>10</sub> and NO<sub>2</sub> at ambient and kerbside and their correlation in Metro City-Mumbai. *Environ. Monitor. Assess.* **119**, 191–199 (2006).
58. Villeneuve, P. J. & Goldberg, M. S. Methodological considerations for epidemiological studies of air pollution and the SARS and COVID-19 coronavirus outbreaks. *Environ. Health Perspect.* **128**, 095001 (2020).

## Acknowledgements

Man Sing Wong thanks the funding support from a grant by the General Research Fund (Grant no. 15602619), the Collaborative Research Fund (Grant no. C7064-18GF), and the Research Institute for Sustainable Urban Development (Grant no. 1-BBWD), the Hong Kong Polytechnic University. Mei-Po Kwan was supported by grants from the Hong Kong Research Grants Council (General Research Fund Grant no. 14605920; Collaborative Research Fund Grant no. C4023-20GF) and a grant from the Research Committee on Research Sustainability of Major Research Grants Council Funding Schemes of the Chinese University of Hong Kong. Hanfa Xing thanks the funding support from a grant by the National Natural Science Foundation of China (Grant no. 41971406). Kai Qin thanks the funding support from a grant by the National Natural Science Foundation of China (Grant no. 41975041).

### Author contributions

Y.M. and M.S.W. had the idea for the study and contributed to study design. Y.M. and K.Q. coordinated data acquisition and standardization. Y.M. analyzed data, interpreted data, and wrote the manuscript. Y.M., H.X., M.P.K., R.Z. and K.H.L. contributed to revision of the manuscript. C.Y.T.K. and H.L. provided administrative, technical, and material support. M.S.W. designed and supervised overall study implementation and obtained funding.

### Competing interests

The authors declare no competing interests.

### Additional information

**Supplementary Information** The online version contains supplementary material available at <https://doi.org/10.1038/s41598-021-91236-w>.

**Correspondence** and requests for materials should be addressed to M.S.W.

**Reprints and permissions information** is available at [www.nature.com/reprints](http://www.nature.com/reprints).

**Publisher's note** Springer Nature remains neutral with regard to jurisdictional claims in published maps and institutional affiliations.



**Open Access** This article is licensed under a Creative Commons Attribution 4.0 International License, which permits use, sharing, adaptation, distribution and reproduction in any medium or format, as long as you give appropriate credit to the original author(s) and the source, provide a link to the Creative Commons licence, and indicate if changes were made. The images or other third party material in this article are included in the article's Creative Commons licence, unless indicated otherwise in a credit line to the material. If material is not included in the article's Creative Commons licence and your intended use is not permitted by statutory regulation or exceeds the permitted use, you will need to obtain permission directly from the copyright holder. To view a copy of this licence, visit <http://creativecommons.org/licenses/by/4.0/>.

© The Author(s) 2021